Creep behavior of gold thin films investigated by bulge testing at room and elevated temperature

Benoit Merle[a)]
Materials Science & Engineering, Institute I, Friedrich-Alexander-Universität Erlangen-Nürnberg (FAU), Erlangen D-91058, Germany

(Received 1 June 2018; accepted 20 July 2018)

The creep behavior of 200-nm thick gold films was investigated by plane-strain bulge testing between 23 and 100 °C. The polycrystalline gold films were produced by thermal evaporation and their columnar microstructure was stabilized by a preliminary heat treatment at 120 °C. The creep tests were performed at constant stress values between 80 and 300 MPa over 12 h, using a custom-built bulge tester. The stress exponent calculated from the creep data decreased from 4.3 to 2.8 between 23 and 100 °C, suggesting a possible transition in deformation mechanisms. The stress exponent and activation energy measured around room temperature point toward the climb of dislocations at grain boundaries being the rate-limiting deformation mechanism. Above 75 °C, scanning electron microscope inspections of tested membranes suggest an increased contribution of diffusion and of grain-boundary mediated deformation, as evidenced by the formation of grooves along grain boundaries. This is presumably the reason for the decrease of the apparent stress exponent and sudden increase of the apparent activation energy.

Benoit Merle

Benoit Merle is leading the research group on nanomechanics and thin film mechanics at the Materials Science & Engineering Department of the University of Erlangen-Nürnberg (FAU), Germany. He obtained his Master of Engineering degree from the Ecole Centrale de Lyon in France in 2005. After spending a few years as an engineer with Siemens AG, he joined the University of Erlangen-Nürnberg to pursue a Ph.D. on the mechanical behavior of thin films, which he completed in 2013. He received a Young Researcher Award from the German Materials Society in 2013 as well as a Ph.D. award by the Staedtler Foundation. His current research focusses on the development of small scale methods enabling the local measurement of mechanical properties, which he uses for investigating mechanical size effects. This research involves thin film specific methods, such as bulge testing or in situ tensile testing, and nanoindentation-based methods, such as micropillar compression and microbeam bending.

I. INTRODUCTION

Knowledge about the creep properties of metallic freestanding thin films is still scarce.[1–7] This is especially true for the lower submicrometric range, due to the fragility[8] of the corresponding specimens, which makes their production and testing extremely challenging. This lack of data is detrimental to the design of reliable microchips and MEMS based on freestanding thin films. Mechanical creep is especially a critical issue for the radiofrequency microswitches providing essential signal processing functionalities to smartphones and other telecommunication systems.[9,10]

The investigations presented in this publication rely on plane-strain bulge testing,[11] which is generally considered a robust method for characterizing specimens as thin as ~40 nm.[12,13] Its reliability is connected to the large area of the tested samples, which limits the statistical effects that can otherwise occur with the much smaller microtensile specimens.[14] As early as 1975, bulge testing was considered suitable for creep testing purposes[15] and several groups have since been actively using it to investigate the time-dependent deformation of thin films.[16–22] Some of these investigations have been performed at elevated temperatures[17,18,20,22] for the purpose of reproducing the operational conditions of the films used in microchips and MEMS. In this study, these technical possibilities are combined in a systematic way in order to characterize the time-dependent properties of gold thin films as a function of the applied pressure and temperature.

[a)]Address all correspondence to this author.
e-mail: benoit.merle@fau.de
DOI: 10.1557/jmr.2018.287

© Materials Research Society 2018. This is an Open Access article, distributed under the terms of the Creative Commons Attribution licence (http://creativecommons.org/licenses/by/4.0/), which permits unrestricted re-use, distribution, and reproduction in any medium, provided the original work is properly cited.

https://doi.org/10.1557/jmr.2018.287 Published online by Cambridge University Press

II. MATERIALS AND METHODS

A. Samples

The investigated samples are 200 nm thick gold films produced by thermal deposition, using a custom built thermal coater operated at a base pressure of 2×10^{-7} mbar. Rectangular 1 mm × 4 mm SiN_x membranes purchased from Silson Ltd. (Southam, U.K.) were used as sacrificial substrates. They consisted of a 100 nm thick SiN_x film held by a 525 μm thick silicon frame. Gold was deposited at a rate of 1–1.5 Å/s onto the SiN_x substrates while these were heated to 80 °C and constantly rotated. The substrates were preheated for 1 h prior to deposition. Following deposition, the films were heat treated at 120 °C for 2 h without interrupting the vacuum, in order to stabilize the microstructure before mechanical testing. A representative image of the resulting microstructure is shown in Fig. 1(a). An evaluation of several electron micrographs by the line intersection method evidenced a mean grain size of 220 ± 13 nm, which is slightly larger than the film thickness. This is in line with the expectation of a mostly columnar microstructure from the Grovenor deposition model.[23] As expected for thermally grown submicron films,[24] the samples also evidenced a strong (111) texture, see Fig. 1(b).

In a further processing step, the SiN_x substrate layer was removed by reactive ion etching using a 30 sccm flow of CF_4 at a pressure of 12.67 Pa and a RF power of 100 W for 3 min. This left the gold film freestanding inside the 4 × 1 mm rectangular opening and ready to be mechanically deformed by bulge testing.

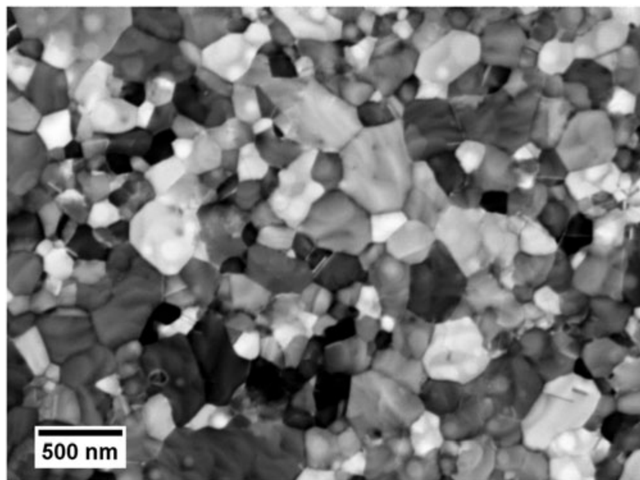

(a)

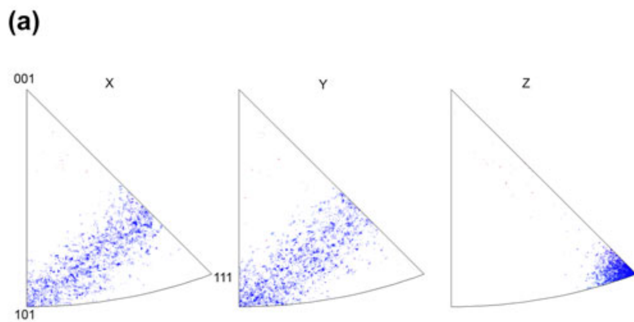

(b)

FIG. 1. Microstructure of the gold films before creep testing: (a) Back-scattered electron micrograph (CrossBeam 540, Zeiss, Germany)—(b) Inverse pole figures from EBSD (Electron Back-Scattered Diffraction, NanoLys Detector, Oxford Instruments, UK) showing a strong (111) texture.

B. Bulge testing

The plane-strain bulge test is a convenient method for measuring the mechanical behavior of thin films. Vlassak et al. showed that the lateral stress σ and strain ε in the sample are directly related to deflection h of the membrane under the action of a given pressure p[11,25]:

$$\sigma = \frac{pa^2}{2ht} \quad , \tag{1}$$

$$\varepsilon = \frac{2h^2}{3a^2} + \varepsilon_0 \quad . \tag{2}$$

The custom-built bulge tester used for this study is shown in Fig. 2. It relies on pressurization by a continuous flow of gaseous nitrogen and a measurement of the resulting deflection by white light interferometry. For the purpose of the present study, a set of miniature heater and thermocouple (Allectra GmbH, Berlin, Germany) was fitted to the sample holder and operated with a PID controller (Eurotherm, Worthing, UK). This combination ensured that the sample could be kept at any temperature in the range 23–110 °C with variations smaller than 0.1 °C during an experiment. The actual temperature of the sample was furthermore calibrated with a reference thermocouple before the beginning of the study. For the

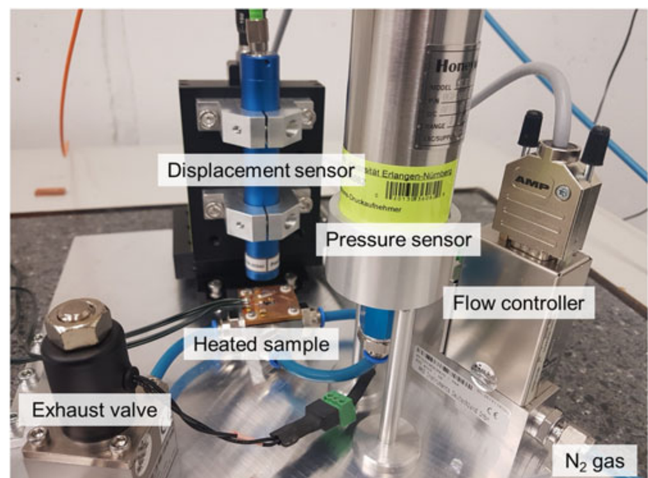

FIG. 2. Custom-built bulge tester for thin films.

https://doi.org/10.1557/jmr.2018.287 Published online by Cambridge University Press

purpose of the creep tests, the bulge tester was confined inside a double-walled enclosure and left to stabilize thermally for 12 h before every creep test so that the measurements would not be affected by thermal drift due to the expansion of the setup.

A supplementary challenge associated with bulge tests at elevated temperature is related to metallic membranes usually becoming slack when heated up, due to their thermal expansion coefficient being much larger than that of the retaining silicon frame. This is usually a critical issue for performing bulge tests because the evaluation procedure requires knowledge of the initial flat position of the membrane. Fortunately, Ghanem et al.[26] have recently shown that measuring the initial height of the central buckle and subtracting it from the displacement data yields robust results, as long as the buckling is not too strong and the pattern disappears upon loading to a certain pressure, as was the case in the present study. As a consequence, the height of the buckle was measured by a line scan using the white light interferometer and its value was taken into account for setting up the creep tests and evaluating the corresponding data.

C. Creep testing

To carry out the creep tests, a feedback loop was implemented into the pre-existing Labview control program. It aimed at continuously adjusting the pressure p to keep the stress σ [Eq. (1)] equal to the value specified by the operator. This required a prior measurement of the geometrical dimensions of the sample and the height of the central buckle. The stress was held constant for a duration of 12 h, during which the load–displacement data were recorded at a rate of 5 Hz. Due to the limited availability of the samples, stress increments of at least 100 MPa were implemented so as to probe the creep response at more than one stress level for each sample and therefore maximize data collection. This procedure is commonly used in macroscopic creep testing.[27] On thin film samples, the repeated loading scheme was found to be unproblematic,[28] as long as the films had been previously annealed and the stress increments were large enough. This holds true for the present study, where samples tested with and without prior stress increment experienced similar creep rates. All in all, 23 similar gold membranes were subjected to bulge creep tests.

The raw load–displacement data were converted to stress–strain data using a Python/SciPy script based upon the analytical model from Vlassak et al. [Eqs. (1) and (2)]. In the next step, the strain data were smoothed and differentiated using a Savitzky–Golay numeric filter[29] associated to a moving window of 1200 s. The effect of the smoothing and differentiating procedures implemented in the Python/SciPy script is illustrated in Fig. 3. The outcome of a measurement is a strain-rate plot where one data point corresponds to 600 s creep data. From this plot, the minimum creep rate can be identified and used as the main parameter extracted from the creep experiment.

III. RESULTS

A. Apparent stress dependence

Measuring the dependence of the creep rate on the applied stress is usually an efficient way to identify the rate-limiting deformation. This is achieved by comparing the experimental values to the theoretical equations derived for most mechanisms.[30] The experimental data from the creep tests on the 23 specimens are displayed as Norton plots in Fig. 4(a). For each investigated temperature, the diagram describes the dependence of the creep rate on the applied stress. Within the limits of the experimental scattering, these data seem to be fairly linear within the investigated stress range. The slope of the linear regression corresponds to the apparent creep stress exponent n for this range:

$$n = \frac{\partial \ln \dot{\varepsilon}}{\partial \ln \sigma} \quad . \qquad (3)$$

The measured stress exponents n are plotted versus the testing temperature in Fig. 4(b). Their value decreases from a maximum of 4.3 at room temperature, to

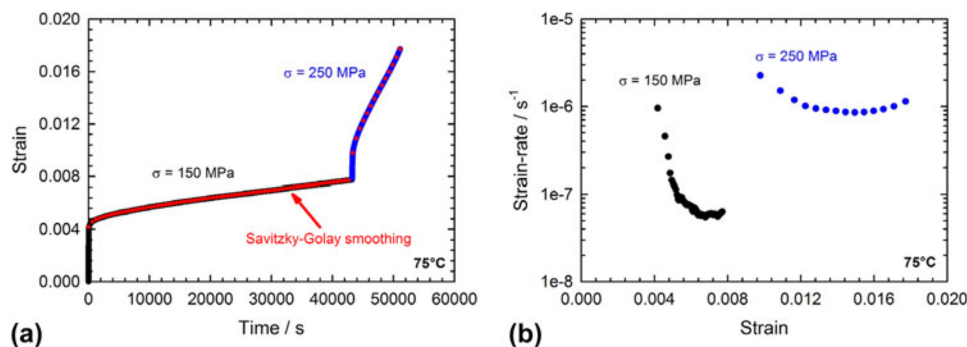

FIG. 3. Smoothing of the strain data by using a Savitzky–Golay numeric filter: (a) Strain data with overlayed smoothened signal—(b) Resulting strain-rate data. The sample shattered during the creep test at 250 MPa, which is why the strain-rate increases toward the end of the measurement.

https://doi.org/10.1557/jmr.2018.287 Published online by Cambridge University Press

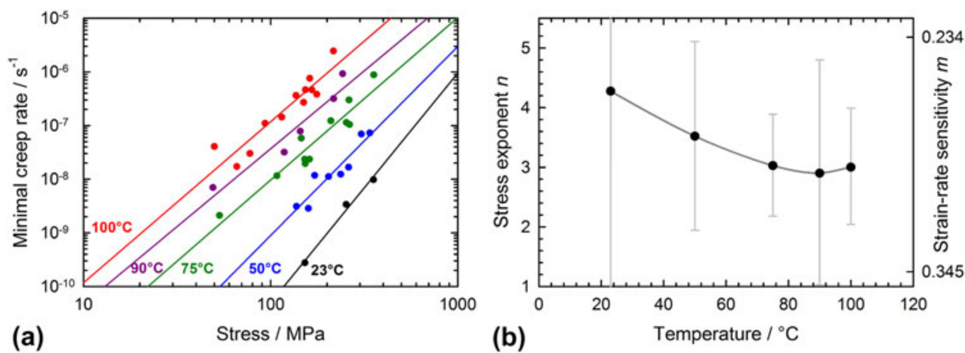

FIG. 4. Apparent stress dependence of the creep of the gold films: (a) Norton plot for each tested temperature, (b) Resulting creep stress exponents as a function of the testing temperature. The error bars correspond to the bounds of the 95% confidence interval of the linear regression.

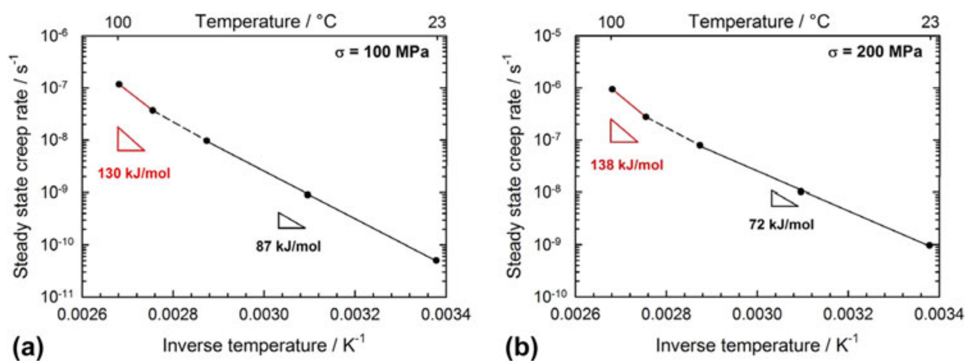

FIG. 5. Arrhenius plots contructed from the interpolated creep data shown in Fig. 4(a) for different creep stresses: (a) 100 MPa—(b) 200 MPa. The apparent activation energy in kJ/mol is calculated by multiplying the slope by R ln 10×10^{-3}.

a minimum of approximately 3 at 75 °C and above, which suggests a change of deformation mechanism occurring around 75 °C. However, it should be pointed out that the experimental scattering of the creep data is significant, as indicated by the large confidence intervals shown in Fig. 4(b). Most of the measured values fall within the characteristic 3–5 range of power-law creep, which is a much-investigated deformation behavior based on dislocation glide and/or climb.[30,31]

B. Apparent temperature dependence

Further information about the creep mechanisms can be inferred from the measurement of the apparent activation energy (also called Gibbs free energy). For this purpose, an Arrhenius plot has to be constructed for a given applied stress, based on the interpolated experimental data previously presented in Fig. 4(a). Calculations for 100 and 200 MPa are shown in Fig. 5. Assuming the most general activation law[32]

$$\dot{\varepsilon} = \dot{\varepsilon}_0 \cdot e^{-\frac{U(\sigma)}{kT}} \quad , \tag{4}$$

the apparent activation energy U can be calculated from the slope of the Arrhenius plots (see Fig. 5). For both investigated stress levels, it appears to remain constant between 23 and 75 °C and subsequently increases to a larger value of 130–140 kJ/mol.

A similar analysis was performed for the whole range of investigated stresses and the corresponding apparent activation energies are summarized in Fig. 6. It is striking that the apparent activation energy depends strongly on the sample temperature and only weakly on the applied stress. This confirms the previous suggestion from the stress exponent analysis that the elevation of the temperature above 80 °C is the main driving force for a transition in deformation mechanisms. The apparent activation energy at room temperature is much smaller than the activation energy for lattice diffusion in gold (167 kJ/mol[33]) but on the order of grain boundary self-diffusion (85 kJ/mol[34]) or surface diffusion (87 kJ/mol[35]). This does not conflict with the previous assumption of diffusion-assisted power-law creep at room temperature. Indeed, while power-law creep is often considered the consequence of dislocations overcoming obstacles inside the grains by climb or glide,[30] it has already been suggested that the annihilation of dislocation pile-ups by climb at the grain boundaries produces similar effects.[36,37] In this case, the measured activation energy corresponds to the diffusion of vacancies along grain boundaries, as it is the case here. The weak

https://doi.org/10.1557/jmr.2018.287 Published online by Cambridge University Press

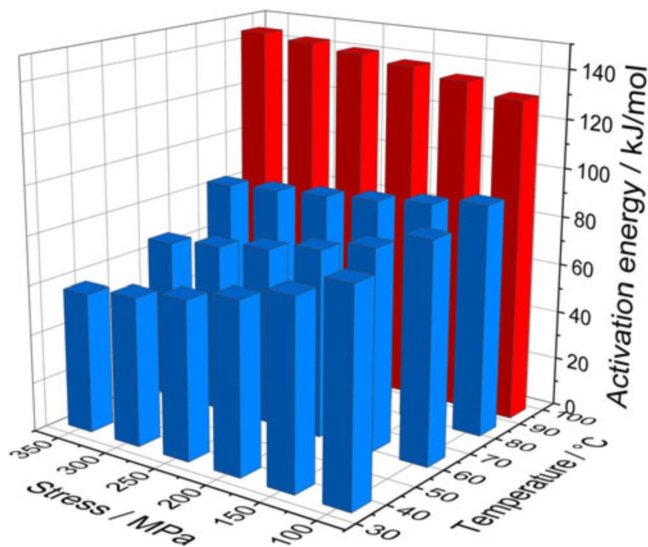

FIG. 6. Calculation of the apparent activation energy for the whole range of investigated stresses. A steep increase is visible around 90 °C.

dependence of the activation energy on the applied stress also visible in Fig. 6 is in no way comparable to the temperature effect. At low temperatures, its small decrease could be interpreted as an indication of the beginning of a transition to dislocation glide at higher stress levels, which is characterized by a lower apparent activation energy.[38]

The measurement of the apparent activation energy values only provides a preliminary hint at the deformation mechanism. Based on these first observations, it is necessary to compare the experimental results to the rate equations predicted by specific models available in the literature.

C. Comparison to stress activation rate-equation

The Arrhenius analysis shown in Fig. 6 hints at a strong influence of the temperature on the kinetics of creep. A popular model is often used to describe such creep deformation, which assumes that dislocations overcoming discrete obstacles by thermal activation[30] or that the thermal activation of Frank–Read sources[32] is the rate-controlling process, in which case the following rate-equation should apply:

$$\dot{\varepsilon} = \dot{\varepsilon}_0 \cdot e^{-\frac{U_0 - V\sigma}{kT}} \quad , \tag{5}$$

where U_0 is the activation energy at 0 K and V is the so-called activation volume. Given the widespread (and sometimes indiscriminate) use of this equation, it is worth taking the time to examine how well it matches the experimental data.

The first step consists of measuring the apparent activation volume as

$$V = kT \frac{\partial \ln \dot{\varepsilon}}{\partial \sigma} \quad . \tag{6}$$

This yields values of the order of b^3, which steadily increase with the testing temperature, see Fig. 7(a). However, as advocated in some textbooks,[39] caution should be taken not to over-interpret the physical meaning of the activation volume and use it to identify a rate-limiting deformation mechanism. Comparison to literature values is also difficult due to the different definitions used by different researchers: V is defined as a derivative either with respect to the resolved shear stress or to the applied tensile stress [as in Eq. (6)]. In the case of a polycrystal, this leads to a difference of a factor 3.06 (Taylor factor[30,40,41]) between the different numerical values reported in the literature. Further adding to confusion, the analysis in certain publications incorrectly assumes a value of $\sqrt{3}$ for the Taylor factor, see discussion in Ref. 42. Altogether, this makes the interpretation of activation volume values and their comparison to the literature a very challenging task.

More importantly, the measurement of the activation volume enables calculating the activation energy at 0 K by subtracting the product $V\sigma$ from the previously measured [Fig. 6(b)] apparent activation energy. The new athermal values are shown in Fig. 7(b). They can readily be compared to the product μb^3 (390 kJ/mol at room temperature, with μ: shear modulus, b: Burgers vector), to gain physical information about the kind of obstacles encountered by the dislocations.[30] The measured $U_0/\mu b^3$ ratio of 0.1–0.2 at room temperature is indicative of a rather weak obstacle strength. This is consistent with the fact that pure gold films do not contain precipitates.

It can be observed for any given stress that the activation energy at 0 K is strongly increased above a temperature of 80 °C. A similar trend also holds for the activation volume [see Fig. 7(a)]. The end of the stability for both parameters evidences that the discrete obstacle thermal activation model described by Eq. (5) breaks down for these temperatures. This strongly suggests that another mechanism is taking over. To characterize its nature, it is necessary to resort to direct observations of the corresponding deformation.

D. Observation of deformation

Only very few gold film specimens survived the creep tests and did not delaminate from the surface when unmounted from the bulge tester. They were inspected in electron backscattering mode (BSD), to be compared with the initial microstructure of the films (shown in Fig. 1). A few representative images taken after the creep tests are shown in Fig. 8. The mean grain size was measured by the line intersection method from at least

https://doi.org/10.1557/jmr.2018.287 Published online by Cambridge University Press

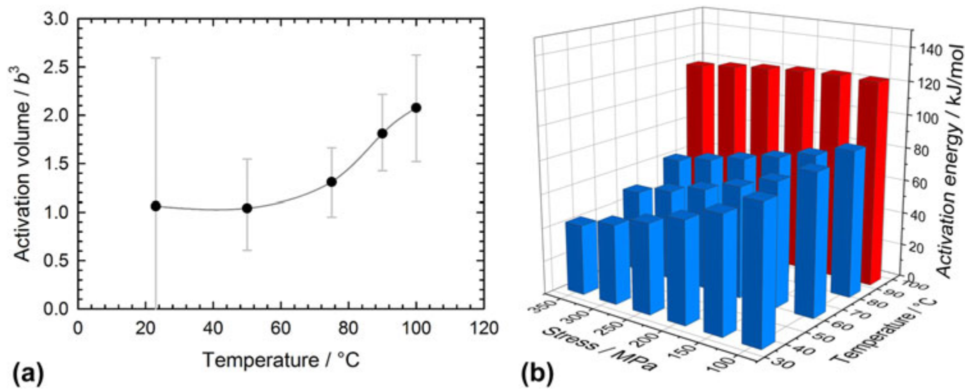

FIG. 7. Evaluation of creep data assuming a dislocation-based discrete obstacles thermally activated limiting mechanism: (a) Activation volume (calculated with respect to σ) with 95% confidence intervals—(b) Activation energy at 0 K.

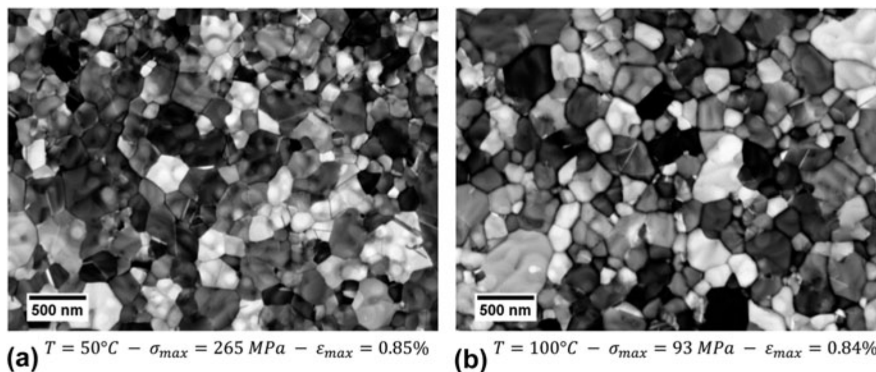

FIG. 8. Morphology of the samples after the creep tests investigated in electron-backscattered contrast (BSD): (a) Sample tested at 50 °C—(b) Sample tested at 100 °C, with similar accumulated strains. After testing at 100 °C, prominent grooves are apparent along the grain boundaries.

four of such micrographs of the same sample. The measurements evidenced no significant growth during testing. For instance, for the samples presented in Fig. 8, mean grain sizes of 223 ± 13 nm and 225 ± 13 nm were found, which do not significantly differ from the pre-creep-test condition (220 ± 13 nm). This is not excessively surprising because the samples were heat treated at 120 °C prior to the tests to ensure that the microstructure would remain thermally stable. Besides, the limited strain (<1%) accumulated during the tests makes it unlikely that any very large mechanically induced grain growth takes place. However, it cannot totally be excluded that grain boundary motion takes place on a limited scale during the creep tests, which cannot be resolved due to technical limitations.

Qualitatively, there appears to be a major difference between the topology of the samples shown in Fig. 8. While the sample tested at 50 °C [Fig. 8(a)] shows little differences to the microstructure pre-existing creep testing (Fig. 1), the sample tested at 100 °C [Fig. 8(b)] evidences dark bands between its grains in electron-backscattered (BSD) contrast. Closer examination reveals that these bands correspond to grooves, which amount to a local thickness reduction. This is not simply a consequence of the accumulated deformation, as both samples shown in Fig. 8 have been tested to a similar total strain. Rather, this appears to be an effect of the temperature since such prominent grain boundary grooves are only found in samples tested above 75 °C. As this temperature range correlates well with the variations in stress exponent and activation energy reported earlier, it appears likely that these are directly connected to the localization of the deformation at grain boundaries.

IV. DISCUSSION

A. Overall deformation behavior

The analysis of the data shown above allows drawing some likely conclusions about the mechanisms governing the deformation of the films at the investigated temperatures and strain-rates. At low temperatures (23–75 °C), the stress exponent analysis points toward a power-law like mechanism. The apparent activation energy value suggests that it relies on the diffusion of vacancies along grain boundaries (or surface). From this, it can be inferred that climbing of dislocations at the grain boundaries is the

https://doi.org/10.1557/jmr.2018.287 Published online by Cambridge University Press

limiting mechanism. This is consistent with in situ TEM observations showing the annihilation of dislocations at the grain boundaries of samples of similar grain size.[43] In any case, the deformation is well described by a discrete obstacle thermal activation model up to a temperature of 75 °C.

In the high temperature range (90–100 °C), the creep data consistently suggest that another rate-controlling mechanism takes over. Although the stress exponent remains constant around 3—which could still correspond to power-law creep—there is a clear break-down from the discrete obstacles thermal activation model. Post-mortem micrographs also evidence a transition to a completely different morphology of the surface of the tested specimens, which is characterized by large grooves running along grain boundaries. The increase of the apparent activation energy to values significantly larger than for grain boundary diffusion might suggest that diffusion along grain boundaries happens much more easily, while the more demanding diffusion of vacancies from the bulk of the grains to their periphery is for some reason required and thus becomes the new rate-limiting mechanism. Deformation by pure diffusion is, however, not consistent with the measured stress exponent value ($n = 1$, even in the case of coatings[44] versus $n = 3$, experimentally) and the described mechanism would presumably restrict grooving to the grain boundaries perpendicular to the main tensile direction, in opposition to the microscopic observations. This suggests that the localized deformation observed at grain boundaries is more likely connected to the accommodation of the shape of the grains required by a structural grain-boundary mediated mechanism, such as grain rotation,[45] grain-boundary sliding,[28,46,47] or shear-coupled grain boundary migration.[48–51] It is quite true that the measured stress exponent values are slightly too high for these mechanisms, as diffusion-supported grain boundary sliding is for instance usually associated with a stress exponent $n \approx 2$.[52] Nonetheless, it should not be overlooked that the underlying model was developed for bulk materials and neither takes into account the possible out-of-plane motion of grains in thin films nor their local thinning and their effect on the overall strain and strain-rate. It is also possible that several mechanisms almost equally contribute to the deformation so that the apparent stress dependency is in fact of a composite value.

B. Comparison to prior studies

The experimental results are partly in agreement with and partly in apparent contradiction to the limited literature available on the creep of thin films.

Karanjgaokar et al. investigated the creep of gold films in the same temperature range[28] as the present work and also observed a transition in deformation mechanisms. They measured similar stress exponent values (in the 3–5 range) but evidenced a different trend, with the stress exponent increasing with temperature. Hence, they concluded that the deformation shifts from grain boundary sliding at room temperature to dislocation power-law creep at 110 °C. Surprisingly, the reported apparent activation energy was found to be constant [Fig. 12(a) in Ref. 28]. It was also significantly smaller than in the present study, suggesting that diffusion did not play any major role. It should, however, be noted that the films investigated by Karanjgaokar et al. had a very different microstructure. Not only were the films one order of magnitude thicker ($t = 1.76$ μm versus 200 nm) but also their mean grain size was much smaller ($d = 53$ nm versus 220 nm). As it is well-known from investigations on the superplastic behavior of materials that the temperature and strain-rate ranges where grain-boundary sliding occurs are significantly affected by the microstructure of the samples,[53] the apparent discrepancy between the studies should not be a matter of surprise.

An even finer microstructure was investigated by Ghazi et al.,[18] who performed creep tests on 200 nm thick copper films of 35 nm mean grain size at room temperature and 100 °C. In opposition to both Karanjgaokar et al. and the present study, they concluded from the experimental creep rate data that Coble creep was the dominating mechanism over the whole temperature range. The present observations agree with the importance of grain-boundary diffusion at room temperature, but the larger apparent activation energy rules it out for the tests performed at 100 °C. Besides, the exponent values measured over the whole temperature range rather point toward dislocation-based creep.

These different behaviors evidence important heterogeneities between thin films and emphasize the need for further experimental investigations of their creep behavior, so as to derive a better understanding of the effects of their microstructure.[54] The originality of the present study lays in the strongly columnar character of its microstructure, which implies that almost every grain extends through the whole thickness. The ubiquitous presence of the free surface is known to influence the strength of the samples[55] and is also believed to promote grain-boundary mediated deformation because less accommodation of the neighboring grains is required. The occurrence of grain-boundary sliding has for instance already been reported in detail in a preliminary study at room temperature by the author.[16] The discrepancy between both room-temperature measurements most likely results from significant differences between the gold samples investigated in both studies. As a matter of fact, the earlier results were achieved on non-annealed samples, which also evidenced a much higher surface roughness, with small grain boundary grooves already present in the as-deposited condition.

https://doi.org/10.1557/jmr.2018.287 Published online by Cambridge University Press

V. CONCLUSIONS

All in all, the report presented a new bulge setup developed for creep tests at elevated temperatures, as well as its application to columnar 200-nm thick gold membranes. The creep data enabled the calculation of the stress exponent, apparent activation energy, and activation energy at 0 K. The recorded trends evidence a transition in deformation mechanisms occurring around 75 °C. At low temperatures (23–75 °C), deformation appears to be governed by the diffusion-assisted climb of dislocations at grain boundaries, as indicated by the stress exponent of ~4, the value of the apparent activation energy of ~80 kJ/mol close to grain boundaries self-diffusion and the good fit to the discrete obstacle thermal activation model. Above 75 °C, this model breaks down and the apparent activation energy increases significantly. No clear picture can be derived from the value of the creep parameters, but direct observations of the surface of the deformed samples reveal a pronounced grooving of the grain boundaries. It is therefore suggested that an increased contribution of both diffusion and grain-boundary mediated deformation is the origin of the measured changes in creep parameters. This behavior seems to be specific of the columnar microstructure investigated in the present study and is not found in thicker nanocrystalline films.

ACKNOWLEDGMENTS

The author gratefully acknowledges significant contributions by Eva Preiβ (FAU Erlangen) for building the bulge tester and by Florentina Gannott (MPL Erlangen) for RIE-etching the SiN_x substrate layer below the gold films. B.M. also expresses his sincere gratitude to Jan P. Liebig for helpful discussions about the creep results.

REFERENCES

1. L. Wang and B.C. Prorok: Strain rate dependent behavior of nanocrystalline gold films. In *11th International Congress and Exhibition on Experimental and Applied Mechanics*, Vol. **4** (Society for Experimental Mechanics, 2008); pp. 1854–1859.
2. D.S. Gianola, D.H. Warner, J.F. Molinari, and K.J. Hemker: Increased strain rate sensitivity due to stress-coupled grain growth in nanocrystalline Al. *Scr. Mater.* **55**, 649–652 (2006).
3. M-S. Colla, B. Amin-Ahmadi, H. Idrissi, L. Malet, S. Godet, J-P. Raskin, D. Schryvers, and T. Pardoen: Dislocation-mediated relaxation in nanograined columnar palladium films revealed by on-chip time-resolved HRTEM testing. *Nat. Commun.* **6**, 5922 (2015).
4. R.D. Emery and G.L. Povirk: Tensile behavior of free-standing gold films. Part I. Coarse-grained films. *Acta Mater.* **51**, 2067–2078 (2003).
5. R.D. Emery and G.L. Povirk: Tensile behavior of free-standing gold films. Part II. Fine-grained films. *Acta Mater.* **51**, 2079–2087 (2003).
6. K. Jonnalagadda, N. Karanjgaokar, I. Chasiotis, J. Chee, and D. Peroulis: Strain rate sensitivity of nanocrystalline Au films at room temperature. *Acta Mater.* **58**, 4674–4684 (2010).
7. N. Karanjgaokar, I. Chasiotis, D. Peroulis, and K. Jonnalagadda: Strain rate and creep response of Au and Ni thin films. In *SEM Annual Conference and Exposition on Experimental and Applied Mechanics*, Vol. **4** (Society for Experimental Mechanics, 2009); pp. 2373–2381.
8. E.I. Preiß, B. Merle, and M. Göken: Understanding the extremely low fracture toughness of freestanding gold thin films by in situ bulge testing in an AFM. *Mater. Sci. Eng., A* **691**, 218–225 (2017).
9. G. Gregori and D.R. Clarke: Mechanical creep as a life-limiting factor of radio frequency microswitches. *Appl. Phys. Lett.* **87**, 1–3 (2005).
10. P. Kolis, A.K. Bajaj, and M. Koslowski: Quantification of uncertainty in creep failure of RF-MEMS switches. *J. Microelectromech. Syst.* **26**, 283–294 (2017).
11. Y. Xiang, X. Chen, and J.J. Vlassak: Plane-strain bulge test for thin films. *J. Mater. Res.* **20**, 2360–2370 (2005).
12. H. Javed, B. Merle, E. Preiß, R. Hivet, A. Benedetto, and M. Göken: Mechanical characterization of metallic thin films by bulge and scratch testing. *Surf. Coat. Technol.* **289**, 69–74 (2016).
13. B. Merle and M. Göken: Fracture toughness of silicon nitride thin films of different thicknesses as measured by bulge tests. *Acta Mater.* **59**, 1772–1779 (2011).
14. M. Coulombier, A. Boé, C. Brugger, J.P. Raskin, and T. Pardoen: Imperfection-sensitive ductility of aluminium thin films. *Scr. Mater.* **62**, 742–745 (2010).
15. I.I. Solonovich: Creep mechanisms of condensed polycrystalline films of copper in the range 20–150 °C. *Phys. Met. Metallogr.* **40**, 158–163 (1975).
16. B. Merle, D. Cassel, and M. Göken: Time-dependent deformation behavior of freestanding and SiN_x-supported gold thin films investigated by bulge tests. *J. Mater. Res.* **30**, 2161–2169 (2015).
17. A.J. Kalkman, A.H. Verbruggen, and G.C.A.M. Janssen: High-temperature bulge-test setup for mechanical testing of free-standing thin films. *Rev. Sci. Instrum.* **74**, 1383–1385 (2003).
18. N. Ghazi and J.W. Kysar: Experimental investigation of plastic strain recovery and creep in nanocrystalline copper thin films. *Exp. Mech.* **56**, 1351–1362 (2016).
19. C-H. Lu, S-C. Wu, A-W. Huang, and M-T. Lin: Time and temperature creep behaviour measurement of al and Al–Mg alloy thin films using pressure bulge tests. In *Conference Proceedings of the Society for Experimental Mechanics Series*, Vol. **2** (2017); pp. 149–154.
20. A-W. Huang, C-H. Lu, S-C. Wu, T-C. Chen, R.P. Vinci, W.L. Brown, and M-T. Lin: Viscoelastic mechanical properties measurement of thin Al and Al–Mg films using bulge testing. *Thin Solid Films* **618**, 2–7 (2016).
21. B.E. Alaca, K.B. Toga, O. Akar, and T. Akin: Strain-controlled bulge test. *J. Mater. Res.* **23**, 3295–3302 (2008).
22. K. Mongkolsuttirat, J.R. Smyth, W.L. Brown, and R.P. Vinci: The effect of grain size on viscoelastic relaxation behavior of Au thin films. *Scr. Mater.* **155**, 1–4 (2018).
23. C.R.M. Grovenor, H.T.G. Hentzell, and D.A. Smith: The development of grain structure during growth of metallic films. *Acta Metall.* **32**, 773–781 (1984).
24. C.V. Thompson: Structure evolution during processing of polycrystalline films. *Annu. Rev. Mater. Sci.* **30**, 159–190 (2000).
25. J.J. Vlassak and W.D. Nix: New bulge test technique for the determination of Young's modulus and Poisson's ratio of thin films. *J. Mater. Res.* **7**, 3242–3249 (1992).
26. M. Ghanem, M. Göken, and B. Merle: Plane-strain bulge testing of thin films under compressive residual stresses. *Surf. Coat. Technol.* **327**, 167–173 (2017).
27. A. Bauer, S. Neumeier, F. Pyczak, and M. Göken: Microstructure and creep strength of different γ/γ'-strengthened co-base superalloy variants. *Scr. Mater.* **63**, 1197–1200 (2010).

https://doi.org/10.1557/jmr.2018.287 Published online by Cambridge University Press

28. N. Karanjgaokar and I. Chasiotis: Creep behavior of nanocrystalline Au films as a function of temperature. *J. Mater. Sci.* **51**, 3701–3714 (2016).
29. A. Savitzky and M.J.E. Golay: Smoothing and differentiation of data by simplified least squares procedures. *Anal. Chem.* **36**, 1627–1639 (1964).
30. H.J. Frost and M.F. Ashby: *Deformation-Mechanism Maps* (Pergamon Press, Oxford, United Kingdom, 1982).
31. J. Weertman: Theory of steady-state creep based on dislocation climb. *J. Appl. Phys.* **26**, 1213–1217 (1955).
32. F.R.N. Nabarro and H.L. De Villiers: *The Physics of Creep* (Taylor&Francis, 1995).
33. W. Rupp, U. Ermert, and R. Sizmann: Self-diffusion measurements in gold single crystals between 286 and 412 °C. *Phys. Status Solidi B* **33**, 509–516 (1969).
34. D. Gupta: Grain-boundary self-diffusion in Au by Ar sputtering technique. *J. Appl. Phys.* **44**, 4455–4458 (1973).
35. T-S. Lin and Y-W. Chung: Measurement of the activation energy for surface diffusion in gold by scanning tunneling microscopy. *Surf. Sci.* **207**, 539–546 (1989).
36. F.R.N. Nabarro: Do we have an acceptable model of power-law creep? *Mater. Sci. Eng., A* **387–389**, 659–664 (2004).
37. J.R. Spingarn and W.D. Nix: A model for creep based on the climb of dislocations at grain boundaries. *Acta Metall.* **27**, 171–177 (1979).
38. G.B. Gibbs: The activation parameters for dislocation glide. *Philos. Mag.* **16**, 97–102 (1967).
39. J.P. Hirth and J. Lothe: *Theory of Dislocations* (John Wiley&Sons, 1982).
40. W.F. Hosford: *The Mechanics of Crystals and Textured Polycrystals* (Oxford University Press, 1993).
41. G.I. Taylor: Plastic strain in metals. *J. Inst. Met.* **62**, 307–324 (1938).
42. R.E. Stoller and S.J. Zinkle: On the relationship between uniaxial yield strength and resolved shear stress in polycrystalline materials. *J. Nucl. Mater.* **283–287**(Part I), 349–352 (2000).
43. F. Mompiou, M. Legros, A. Boé, M. Coulombier, J-P. Raskin, and T. Pardoen: Inter- and intragranular plasticity mechanisms in ultrafine-grained Al thin films: An in situ TEM study. *Acta Mater.* **61**, 205–216 (2013).
44. M.D. Thouless, J. Gupta, and J.M.E. Harper: Stress development and relaxation in copper films during thermal cycling. *J. Mater. Res.* **8**, 1845–1852 (1993).
45. P. Liu, S.C. Mao, L.H. Wang, X.D. Han, and Z. Zhang: Direct dynamic atomic mechanisms of strain-induced grain rotation in nanocrystalline, textured, columnar-structured thin gold films. *Scr. Mater.* **64**, 343–346 (2011).
46. M.A. Haque and M.T.A. Saif: Deformation mechanisms in free-standing nanoscale thin films: A quantitative in situ transmission electron microscope study. *Proc. Natl. Acad. Sci. U. S. A.* **101**, 6335–6340 (2004).
47. J. Lohmiller, A. Kobler, R. Spolenak, and P.A. Gruber: The effect of solute segregation on strain localization in nanocrystalline thin films: Dislocation glide versus grain-boundary mediated plasticity. *Appl. Phys. Lett.* **102**, 241916 (2013).
48. D.S. Gianola, S. Van Petegem, M. Legros, S. Brandstetter, H. Van Swygenhoven, and K.J. Hemker: Stress-assisted discontinuous grain growth and its effect on the deformation behavior of nanocrystalline aluminum thin films. *Acta Mater.* **54**, 2253–2263 (2006).
49. T.J. Rupert, D.S. Gianola, Y. Gan, and K.J. Hemker: Experimental observations of stress-driven grain boundary migration. *Science* **326**, 1686–1690 (2009).
50. F. Mompiou, D. Caillard, and M. Legros: Grain boundary shear–migration coupling—I. In situ tem straining experiments in al polycrystals. *Acta Mater.* **57**, 2198–2209 (2009).
51. A. Rajabzadeh, F. Mompiou, M. Legros, and N. Combe: Elementary mechanisms of shear-coupled grain boundary migration. *Phys. Rev. Lett.* **110**, 265507 (2013).
52. H. Lüthy, R.A. White, and O.D. Sherby: Grain boundary sliding and deformation mechanism maps. *Mater. Sci. Eng.* **39**, 211–216 (1979).
53. P. Feldner, B. Merle, and M. Göken: Superplastic deformation behavior of Zn–22% Al alloy investigated by nanoindentation at elevated temperatures. *Mater. Des.* **153**, 71–79 (2018).
54. J.P. Liebig, M. Göken, G. Richter, M. Mackovic, T. Przybilla, E. Spiecker, O.N. Pierron, and B. Merle: A flexible method for the preparation of thin film samples for in situ TEM characterization combining shadow-FIB milling and electron-beam-assisted etching. *Ultramicroscopy* **171**, 82–88 (2016).
55. B. Yang, C. Motz, M. Rester, and G. Dehm: Yield stress influenced by the ratio of wire diameter to grain size—A competition between the effects of specimen microstructure and dimension in micro-sized polycrystalline copper wires. *Philos. Mag.* **92**, 3243–3256 (2012).

https://doi.org/10.1557/jmr.2018.287 Published online by Cambridge University Press